energies

MDPI

Article

Experimental Sensorless Control of Switched Reluctance Motor for Electrical Powertrain System

Ahmed Chaibet [1], Moussa Boukhnifer [2,*], Nadir Ouddah [1] and Eric Monmasson [3]

[1] École Supérieure des Techniques Aéronautiques et de Construction Automobile, ESTACA, 78066 Saint-Quentin-en-Yvelines, France; ahmed.chaibet@estaca.fr (A.C.); nadir.ouddah@gmail.com (N.O.)
[2] Université de Lorraine, LCOMS, F-57000 Metz, France
[3] Génie Électrique et Informatique Industrielle, Université de Cergy-Pontoise, 95000 Cergy-Pontoise, France; eric.monmasson@u-cergy.fr
* Correspondence: moussa.boukhnifer@univ-lorraine.fr

Received: 24 April 2020; Accepted: 2 June 2020; Published: 15 June 2020

Abstract: In this paper a mechanical sensorless control of Switched Reluctance Motors (SRMs) scheme of an electric vehicle (EV) powertrain is presented. The aim is to develop a soft sensors implementation for position and speed measurements of SRM. This contribution is focused on an extended Kalman filter and a sliding mode observer. The proposed observers are designed to generate speed and position estimations with the purpose of achieving highly robust speed control. The performances of these two observers are assessed and their robustness are analyzed. The design also includes a robustness analysis of the proposed mechanical sensorless control scheme under conditions which take the parameter variations and the load torque into account. To carry out this work, experiments are highlighted on an experimental test bench of 8/6 Switched Reluctance Motor prototype.

Keywords: Switched Reluctance Motor; electrical vehicle; robust control; sliding mode observer; extended Kalman filter

1. Introduction

Currently, air pollution is a major concern in our society due to its impact on public health and the environment; for example, road transport accounts for a very large part of greenhouse gas emissions. It therefore becomes essential to find new alternatives to travel, to adopt new transport practices to remedy these environmental problems. The most promising solution for reducing urban traffic congestion, reducing air pollution, and improving the urban environment is the use of electric vehicles. Indeed, the powertrain of an electric vehicle differs significantly from the conventional vehicle. Figure 1 shows the basic configuration of the electric powertrain. This powertrain can be devised into two parts, which are the powertrain system (motor, converter, gearbox, sensors, etc.) and power supply system (battery pack, fuel cell, DC/DC converters, etc.) [1,2].

Many efforts are made in research and development in order to achieve the same level of performance of conventional combustion engine vehicles. To achieve this end, the objective is to adapt to the various constraints linked to the design of electric motors [3,4]. Furthermore, the control of an electric powertrain nevertheless requires precise knowledge of position and speed of the motor shaft. Usually these informations are provided by sensor. There are still a few drawbacks associated with this one. It therefore represents the weak link in the control chain. Indeed, in addition to the size and the difficulty of adaptation and mounting on all types of training, it is delicate and expensive. However, its function can be fulfilled by combining electrical measurements with calculation algorithms to reconstruct of position and speed.

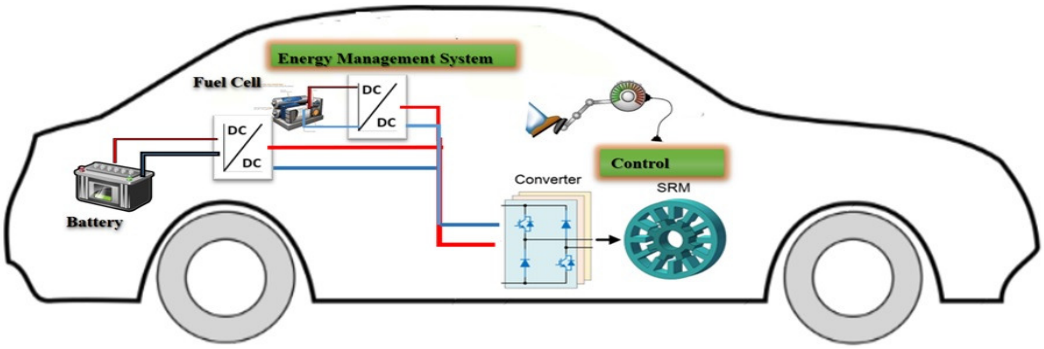

Figure 1. Electric vehicle powertrain system.

In addition, several methods of position estimation have been proposed in the literature [5–10], on how to counter the problems the reliability of the sensors in a complex and hostile operating environment, including electric powertrain . Therefore, designing complete observers (both position and speed estimation) is a necessary step for control tracking, diagnosis, and other fault-tolerant control design problems. Indeed, the expected result is to develop two sensorless control schemes devoted to the electric vehicle (EV) application. For this purpose, an extended Kalman filter observer and sliding mode observer are particularly interesting for EV applications because they are considered more robust observers for rebuilding the state of the Switched Reluctance Motor (SRM) in relation to other estimation techniques. The importance of such a robust state estimation is to ensure high dynamical performance and robustness under various operating conditions needed in an electric vehicle environment.

This work consists of a comparative study between the two observers (sliding mode observer and Kalman filter) in order to benefit from each observer in a wide operating range of vehicle speed. Indeed, the proposed observers are combined with a robust control strategy to reduce the effects of parameter uncertainties and variations and thus ensure high dynamic performance and robustness needed in an electric vehicle environment. Robust H_∞ controllers are designed to enhance the robustness of the overall mechanical sensorless SRM drive system. The errors in speed and robustness analysis against load torque disturbance and parameter variations are presented as well. Moreover, this work will serve as a basis for future work on the position, velocity sensor fault diagnosis, including for further development of the of a fault tolerant control with online reconfiguration using the voting algorithm. The outline of this paper is as follows: Section 2 describes the details of SRM behaviour. Section 3 deals with the encoderless architecture of the SRM. Furthermore, to show the effectiveness of the proposed approach, experimental validation is considered in Section 4. Conclusions are drawn in Section 5 to close this paper.

2. Modeling of Switched Reluctance Motor

The operation mode of SRM motor requires knowing the magnetic position which corresponds to the linking flux as a function of the phase current for the angles of the rotor. These different quantities are essentially obtained either by numerical calculations or by experiments. In this work, we have relied on the Finite Element Method (FEM) which is illustrated in Figure 2. The strong nonlinearity of the magnetic characteristics of the SRM could be introduced in the mathematical model of the motor either, by the use of polynomial interpolations directly provided in a lookup table. It is further considered that the nonlinear electric part of the SRM is represented by curves. However, the mechanical behaviour is described by state space representation.

To analyze and describe the behavior of such motor, a mathematical model is needed. Indeed, the overall behavior of SRM motor can be described by the following equation system [3,10,11]:

$$\frac{di_j}{dt} = \frac{1}{L_{inc}\left(\theta, i_j\right)}\left(V_j - Ri_j - E\right) \quad (1)$$

$$\frac{d\Omega}{dt} = \frac{1}{J}\left(T(\theta, i_j) - T_L - f\Omega\right) \quad (2)$$

$$\frac{d\theta}{dt} = \Omega \quad (3)$$

where:

$$\begin{cases} \phi_j(\theta, i_j) = L_j(\theta, i_j) i_j \\ L_{inc_j} = L_j(\theta, i_j) + i_j \frac{\partial L_j(\theta, i_j)}{\partial i_j} \\ E_j = i_j \Omega \frac{\partial L_j(\theta, i_j)}{\partial \theta} \end{cases}$$

The first Equation (1) corresponds to the electrical equation, while the second one (2) and the last one (3) correspond to the fundamental principle of dynamics of the SRM rotor. The nonlinearity of the magnetic characteristics of the variable reluctance motor could be introduced in the mathematical model of the motor, either by the use of polynomial interpolations directly on the digital data of the flux or of inductance.

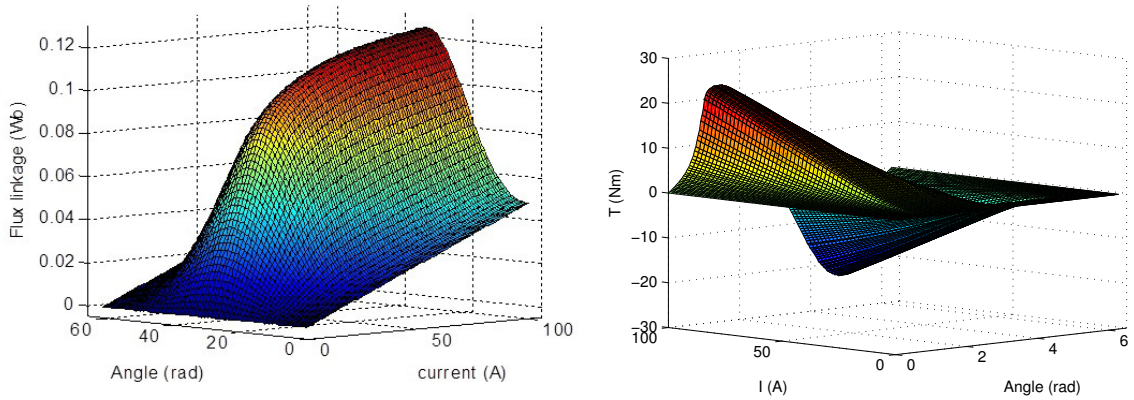

(**a**) (**b**)

Figure 2. Finite Element Method (FEM) flux linkage and static torque curves. (**a**) Flux-linkage. (**b**) Static torque.

3. Sensorless Control Scheme of the SRM

3.1. Design of H_∞ Control

The main motivation consists in developing controllers that are both efficient, easy to implement, and embeddable. To achieve this, emphasis is placed in particular on the design of controllers minimizing the H_∞ norm by taking into consideration the constraints imposed by the electric powertrain application. It is renowned for its performances and robustness properties against parameters uncertainties and disturbance rejection. To design a sensor control scheme of the SRM, one relies on cascaded speed/current loop. Such a strategy has allowed us to eliminate the strong coupling between the electrical and mechanical variables. Furthermore, the control methodology of the inner and outer loop are designed separately [12]. As we can see from Figure 3, the considered cascaded loop consists two nested loops. The first one corresponds to the internal loop (slave loop), aims to control phase currents. The task of the second one, external loop (master loop) is to track the reference SRM speed.

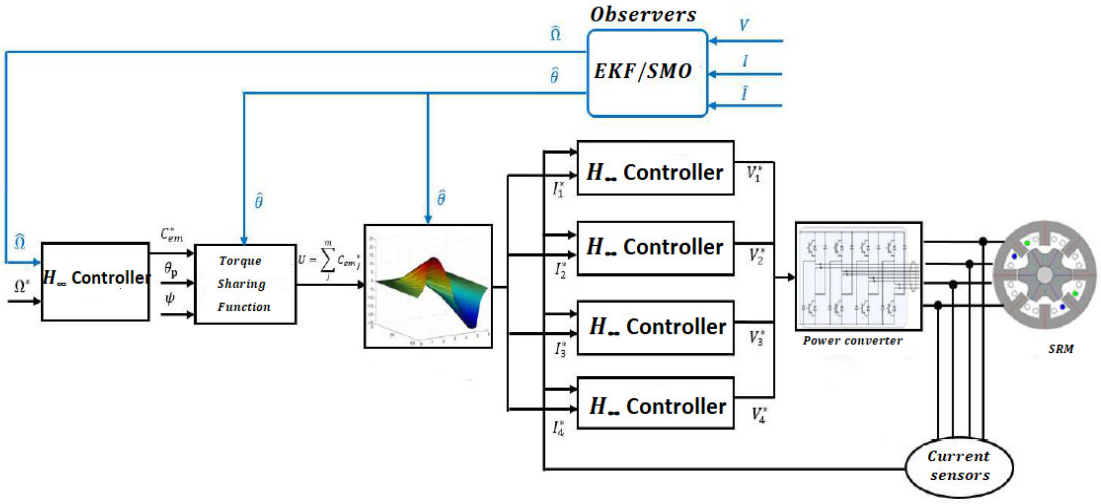

Figure 3. Sensorless speed control Switched Reluctant Motor (SRM) drive scheme.

The remainder of this work is dedicated to the real implementation of robust sensorless control of SRM within an (EV) embedded context which controller order must be taken into account. At this end, the elaboration process of fixed structure H_∞ controller for the studied motor was addressed in detail in a previous work of our team. For more details, interested readers are invited to consult [13,14]. To control the speed and the current loops via the fixed H_∞ approach, we relied on the diagram given in Figure 4 where G corresponds to the mechanical and electrical dynamic, K is the controller, W corresponds to the reference and disturbance signals, Z is related to the outputs which be controlled, W_1, W_2 and W_3 are weighting functions, introduced to ensure trajectory tracking performance, robustness and limitation of the control and disturbance rejection.

- The designed controller $K(\rho)$ is structured with parameter $\rho \in R^n$.
- The purpose is to find γ and compute $K(\rho)$ which stabilizes the system and minimizing the following norm [15]:

$$\|F_L\ (P, K(\rho))\|_\infty = \left\| \left[C_{cl}(K(\rho))\,(sI - A_{cl}(K(\rho)))^{-1} B_{cl}(K(\rho)) + D_{cl}(K(\rho)) \right] \right\|_\infty < \gamma \quad (4)$$

- The resolution of optimization problem (4) is obtained by using a numerical non-convex optimization algorithm.

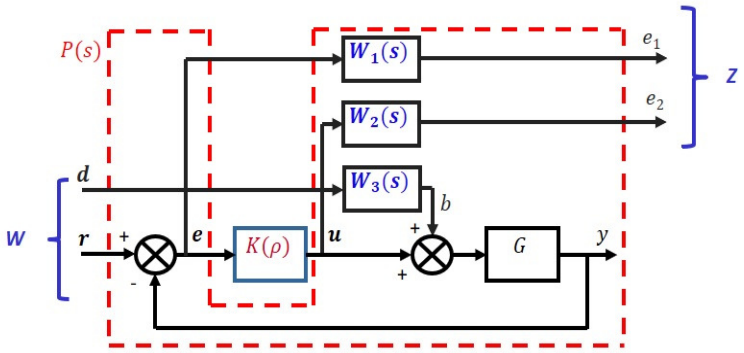

Figure 4. H_∞ design procedure.

3.2. EKF and SMO Observers Design

In this section, we focus on the design and the performances of Extended Kalman Filter (EKF) and Sliding Mode Observer (SMO). The proposed observers were integrated with the robust control

presented above. Comparative study should enable us to assess the performance and robustness of these sensorless control schemes using the estimated of speed and position of SRM. The Extended Kalman Filter (EKF) is based on the merging the measurements and the physical model to build a better estimate of the system's state. EKF estimates the state at time $k+1$ from an estimate at time k and measurements at time $k+1$. The estimation consists of two steps: the first one concerns the state's prediction of the evolution model and while the second one is the correction of the prediction from the measurements. In addition, the Sliding Mode Observer (SMO) is designed from the theory of variable structure systems.

3.2.1. Extended Kalman Filter (EKF)

This paragraph presents the SRM sensorless control design with an Extended Kalman Filter (EKF). Considering the SRM behaviour's given by a system of Equations (1)–(3), a vector format can be deduced in which x corresponds to the state vector, u is the input (measurement) vector and y_p is the output vector: $x = [i_j, \Omega, \theta, T_L]^t$, $y_p = [i_j]^t$ and $u = [V_j]^t$

The system of Equations (1)–(3) can be discretized and rewritten as:

$$\begin{cases} x_{k+1} = f(x_k, u_k) + w_k \\ y_{p_k} = h(x_k) + v_k \end{cases} \tag{5}$$

where f and h are the functions used to compute the predicted state and measurement respectively.

w_k and v_k represent the process and measurement noise with normal probability distributions respectively.

$$\begin{cases} w \sim N(0, Q) \\ v \sim N(0, R) \end{cases} \tag{6}$$

The process noise covariance Q and the measurement noise covariance R are assumed constants.

The Kalman filter has the prediction and the update phases:

The prediction phase uses the estimated state of the previous instant to produce an estimate of the current state. In the update phase, the observations of the current time are used to correct the predicted state in order to obtain a more precise estimate. These different phases are summarized in the Figure 5.

For a straightforward application of this algorithm to the SRM, the observer model can be written from the linearization of (5) as:

$$\begin{cases} \hat{x}_{k+1} = A(\hat{x}_k).\hat{x}_k + B(\hat{x}_k).u_k + K_k.e_k \\ \hat{y}_k = C.\hat{x}_k \end{cases} \tag{7}$$

where $\hat{x}$ is the estimation of x, A, B are the Jacobian matrices of partial derivatives of f with respect to x and to u and C is the Jacobian matrix of partial derivative of h with respect to x respectively.

$$\begin{cases} A_{[n,m]} = \frac{\partial f_{[n]}}{\partial \hat{x}_{[m]}}(\hat{x}_k, u_k) \\ B_{[n,r]} = \frac{\partial f_{[n]}}{\partial u_{[r]}}(\hat{x}_k, u_k) \\ C_{[r,m]} = \frac{\partial h_{[r]}}{\partial \hat{x}_{[m]}}(\hat{x}_k) \end{cases} \tag{8}$$

with $n = m = 7$ and $r = 4$, the elements $a_{[m,n]}$ of matrix A and the matrix B are giving in Appendix A, where T_s is the sampling time. The matrices Q and R are chosen by an iterative method in such a way that the estimation errors are steered towards to zero in finite time and filter stability is ensured. The numerical values of $Q = 1.5 \times 10^{-4}\ I_n$, $R = 4.75 \times 10^{-1}\ I_n$.

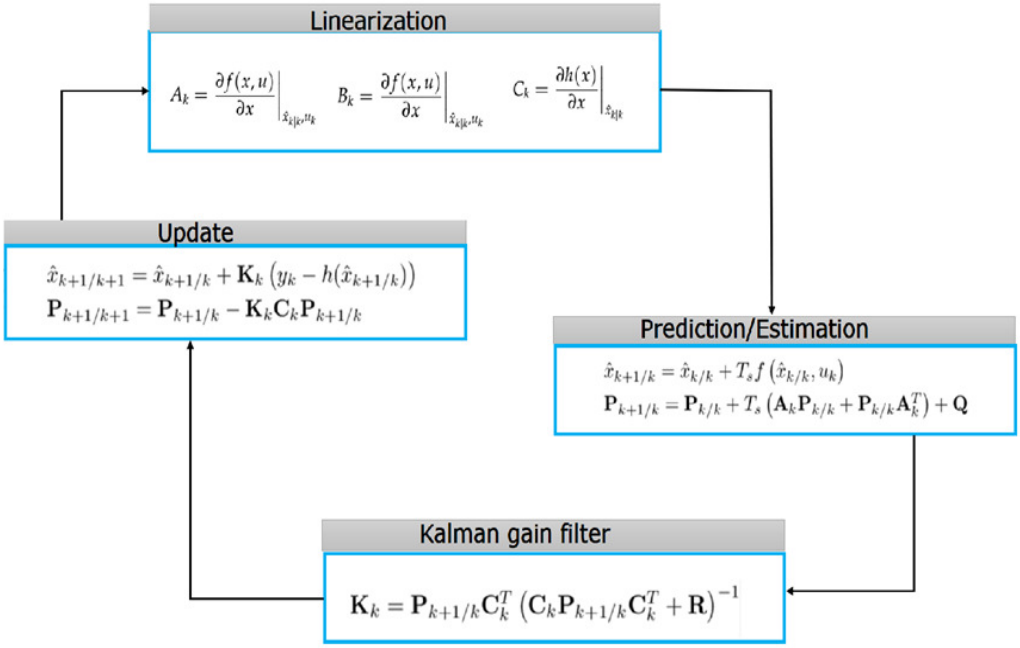

Figure 5. Discrete Extended Kalman Filter block diagram.

3.2.2. Sliding Mode Observer (SMO)

In this subsection, the design of observer for the SRM based on the sliding mode technique is proposed. The aim is to estimate the rotor position and speed. According to the mechanical equations of the nonlinear model of the SRM ((2) and (3)), the sliding mode observer can be defined as follows [16]:

$$\begin{cases} \frac{d\hat{\theta}}{dt} = \widehat{\Omega} + K_\theta |e|^{\frac{1}{2}}.sign(S) \\ \frac{d\widehat{\Omega}}{dt} = \frac{1}{J}\left(\hat{T}(\hat{\theta},\hat{i}) - \hat{T}_L - f.\widehat{\Omega}\right) + K_\Omega.sign(S) \end{cases} \tag{9}$$

where $\hat{\theta}$, $\hat{\Omega}$ and $\hat{T}$ are the estimations of θ, Ω and T respectively. K_θ and K_Ω are the SMO gains. S is the SMO switching surface which compares measured electrical variables with their corresponding estimated values.

The sliding mode observer for SRM can be built that brings the estimation error for all estimated states (position and speed) to steer toward zero in a finite. The sliding surface can be defined as the position observation error.

Now, the first step consists of defining the observation errors:

$$e_\theta(t) = \theta(t) - \widehat{\theta}(t) \tag{10}$$

$$e_\Omega(t) = \Omega(t) - \widehat{\Omega}(t) \tag{11}$$

From (10), the dynamic of the error is:

$$\frac{de_\theta}{dt} = \frac{d\theta}{dt} - \frac{d\widehat{\theta}}{dt} \tag{12}$$

Replacing (9) into (12), we obtain:

$$\frac{de_\theta}{dt} = \Omega - \left(\hat{\Omega} + K_\theta |e|^{\frac{1}{2}}.sign(S)\right) \tag{13}$$

$$\frac{de_\theta}{dt} = e_\Omega - K_\theta |e|^{\frac{1}{2}}.sign\,(S) \tag{14}$$

In the same way as above, we express the error speed dynamic:

$$\frac{de_\Omega}{dt} = \frac{d\Omega}{dt} - \frac{d\widehat{\Omega}}{dt} \tag{15}$$

Substituting the two Equations (2), (3) and (9), we obtain the following equation:

$$\frac{de_\Omega}{dt} = \frac{1}{J}\left[(T(\theta,i) - T_L - f.\Omega) - \left(T(\hat{T}(\widehat{\theta},\hat{i})) - \hat{T}_L - f.\hat{\Omega}\right)\right] - K_\Omega.sign(S) \tag{16}$$

It is assumed that the gain K_Ω is chosen to be large enough so that the first term in Equation (16) can be neglected, the speed error dynamics become:

$$\frac{de_\Omega}{dt} = -K_\Omega.sign(\mathrm{S}) \tag{17}$$

The proposed observer requires that the condition of stability be proven, we give in this work some basic elements of stability proof by using the Lyapunov concept. To ensure the stability of the proposed sliding mode observer, one defines the following function:

$$V_\theta = \frac{1}{2}{e_\theta}^2 \tag{18}$$

The derivative of the (18) is:

$$\dot{V}_\theta = e_\theta \dot{e}_\theta = e_\theta e_\Omega - K_\theta e_\theta sign(S) \tag{19}$$

To keep the function (19) negative, the following conditions must be verified:

- S must have the same sign as e_θ
- $K_\theta > |e_\Omega|$

Therefore, $\dot{e}_\theta$ will have a different sign of e_θ and the estimation error converges to the sliding surface in finite time. When the sliding surface is reached, the speed estimation error e_Ω converges to zero exponentially. To meet these requirements, the surface function is given by the following formula [17]:

$$S = \sum_{j=1}^{N} \sin[\hat{\theta} - (j-1)\,\frac{2\pi}{N_r N}](i - \hat{i}) \tag{20}$$

The discrete time formulation of the sliding mode observer used for real time implementation is expressed using the first-order Euler's approximation as:

$$\begin{cases} \hat{\theta}(k+1) = \hat{\theta}(k) + \left[\hat{\Omega}(k) + K_\theta\,|S|^{\frac{1}{2}}.sign\,(S)\right].T_s \\ \widehat{\Omega}\,(k+1) = \widehat{\Omega}\,(k) + \left[\frac{1}{J}\left(\hat{T} - \hat{T}_L - f.\widehat{\Omega}\,(k)\right) + K_\Omega.sign\,(S)\right].T_s \end{cases} \tag{21}$$

where the estimation errors are:

$$e_\theta\,(k) = \theta\,(k) - \widehat{\theta}(k) \tag{22}$$

$$e_\Omega\,(k) = \Omega\,(k) - \widehat{\Omega}\,(k) \tag{23}$$

The estimation error dynamics are given by the following equations:

$$e_\theta\,(\mathrm{k}+1) = e_\theta\,(\mathrm{k}) + \left(\mathrm{e}_\Omega\,(\mathrm{k}) - K_\theta|e|^{\frac{1}{2}}.sign\,(S\,(k))\right).\mathrm{T_s} \tag{24}$$

$$e_{\Omega}(k+1) = e_{\Omega}(k) - K_{\Omega}.sign(S(k)).T_s \quad (25)$$

where T_s is the sampling time interval which must be smaller than the SRM electrical time constant.

4. Experimental Validation

Extensive laboratory experimental simulations were conducted in different conditions to evaluate strongly the benefits of our study. With the increasing accuracy of SRM machine and the use of standard drive profiles (New European Driving Cycle (NEDC) and/or Extra Urban Driving Cycle (EUDC)). Laboratory experimental simulations (Hardware In the Loop (HIL) approach) have become a valuable step before reel validation. An overview of the experimental platform is depicted in Figure 6. A brief description of this test bench is given in this section. It consisted of Switched Reluctance Motor coupled to an electromagnetic particle brake used as load torque unit, a power inverter (asymmetric half bridge converter), and a dSPACE 1005 control unit with a sampling time of 100 µs. In addition, the test bench was completed by various sensors: a torque transducer to measure the mean torque (Honeywell model: 1104-500, Capacity: 55 Nm), an encoder to measure the angular position and speed of the motor, and 4 Hall effect sensors to measure the electric phase currents.

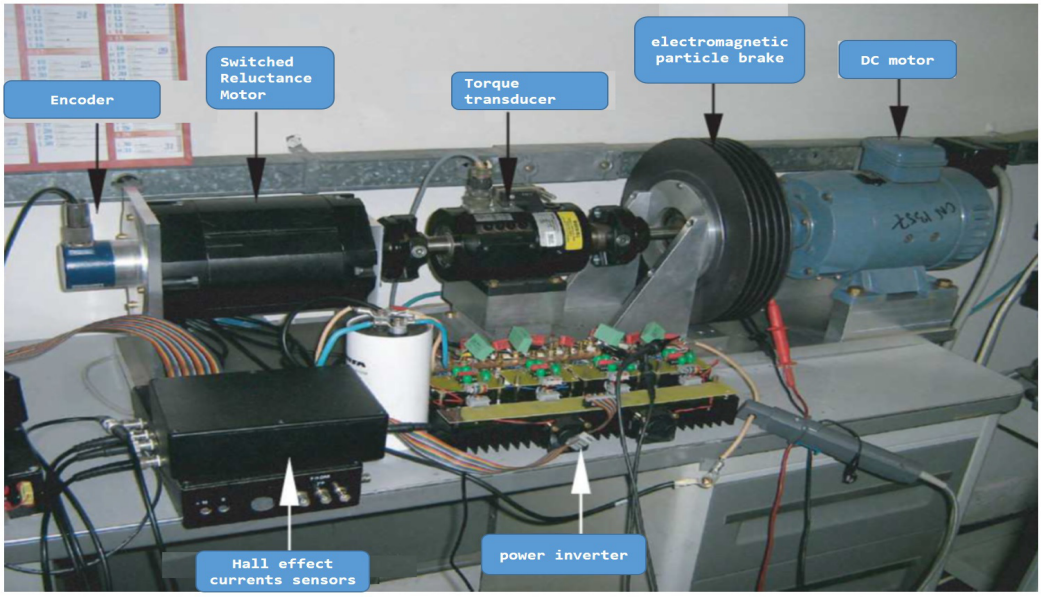

Figure 6. Experimental platform of GeePs Laboratory.

Real time validation was performed to assess the performance and analysis the robustness of SRM speed sensorless. For this purpose, EKF and SMO observers were integrated separately into the control scheme presented in Figure 3. As shown in this figure, only the measurements of electrical variables were used for the control; the position and the speed were provided by observers.

Figure 7 provides an overview of measured and estimated SRM speed profile. This profile consists of different speed steps. From this figure, one can notice that the estimated speed converged asymptotically toward the measured one. Moreover, the obtained performances were good, both in terms of dynamics and in statics. In addition, it can be concluded that the proposed observers presented a good speed tracking performances. However, the sliding mode observer's tracking performances were better than those of the extended Kalman filter at low speed, while the tracking performances of the extended Kalman filter were considerably better at medium and high speed (as shown in Figure 7). A quantitative comparison of these different errors is summarized in the Table 1. Furthermore, the measured and estimated of torque and current are shown in Figure 8.

The obtained performances were good, both in terms of dynamics and in statics.

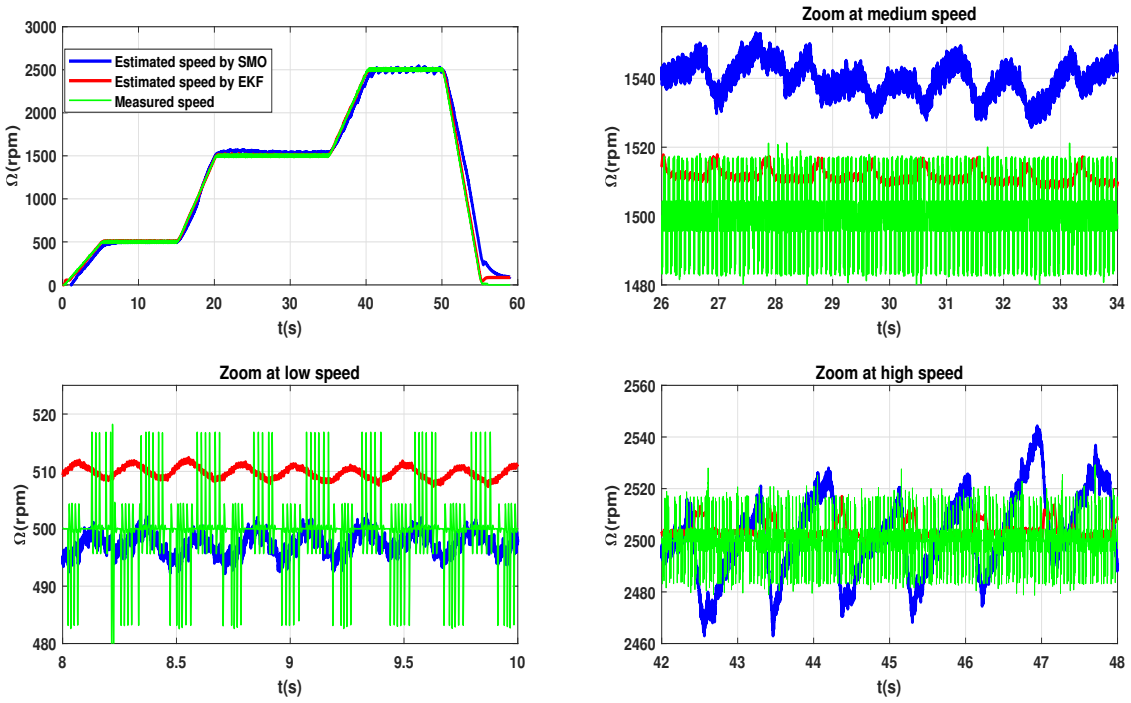

Figure 7. SR motor speed estimation by Extended Kalman Filter (EKF) and Sliding Mode Observer (SMO).

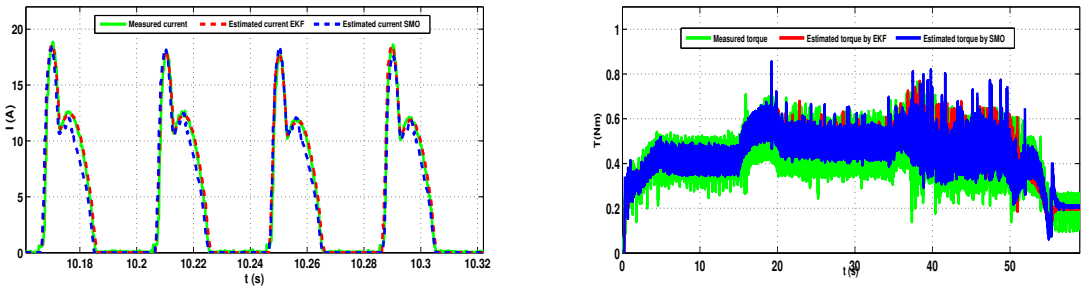

(**a**) (**b**)

Figure 8. Torque estimation and current estimation by EKF and SMO. (**a**) Phase current estimation by EKF and SMO. (**b**) Torque estimation by EKF and SMO.

Moreover, the robustness of the sliding mode observer and the Extended Kalman Filter against load torque disturbances was tested by introducing a load torque variation during steady state. Figure 9a,b illustrate the observer's response to 2.5 Nm of load torque variation. From these figures one can see that the estimated electromagnetic torques evolved accordingly to compensate for the load torque disturbance, which confirms that the two observers were able to track the speed reference trajectory with respect to load torque variation. Furthermore, to demonstrate the robustness of the proposed observers, additional tests were conducted by varying the mechanical and electrical parameters. For this end, the numerical values of the observers design, including the moment of inertia, friction coefficient, the resistance, and self inductance were elevated by 25% compared to their nominal values. The obtained experiments following this test are presented on Figure 9c–f. These figures illustrate the SRM speed responses under the considered robustness. Through analysis of this test, we can notice that the control scheme remained stable. Moreover, the proposed observer's

architecture presented a good reference tracking and ensure the robustness with respect to these parametric variations.

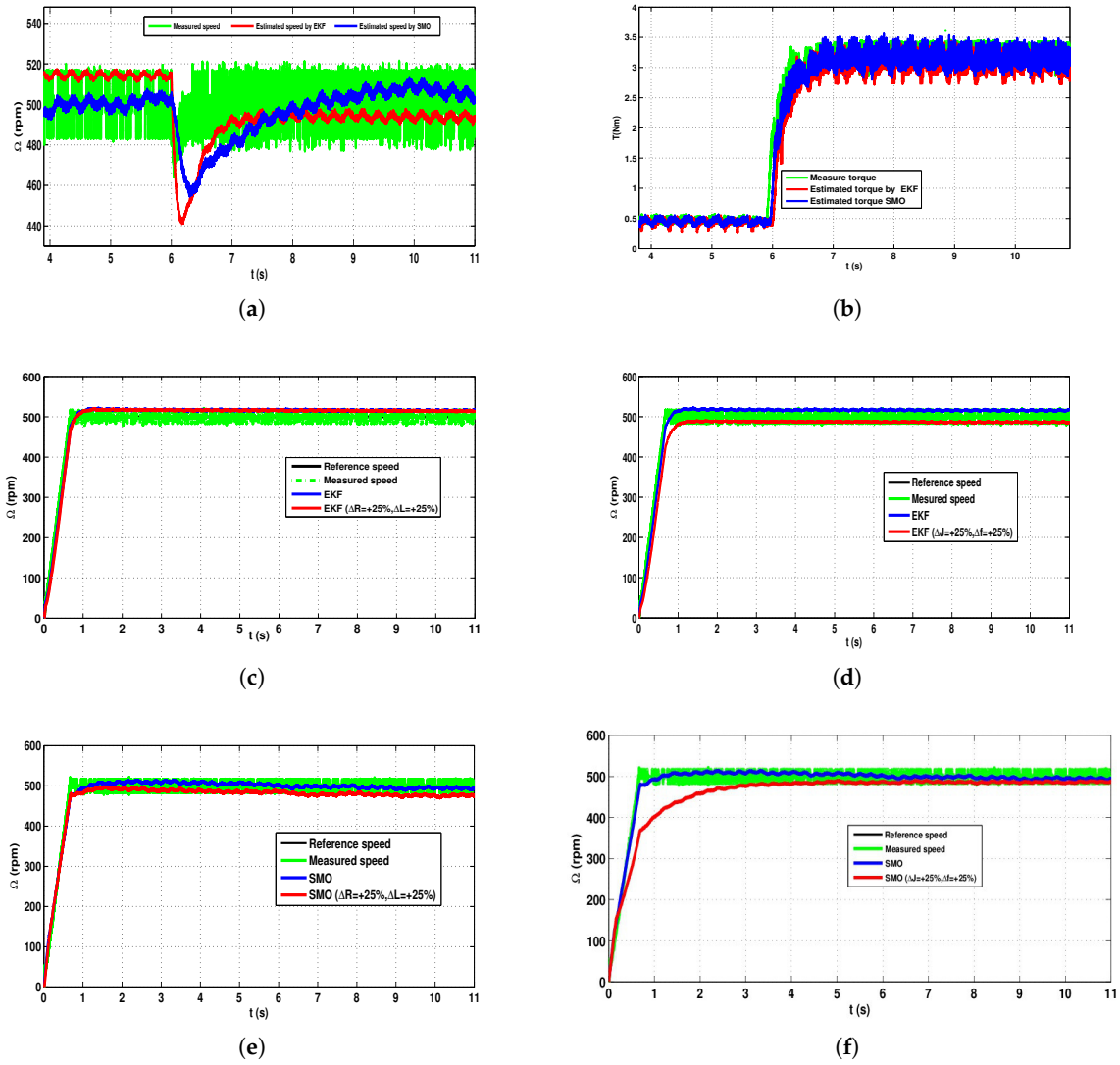

Figure 9. Observers robusteness experiment tests. (**a**) Speed tracking profile against load torque. (**b**) Torque estimation by EKF and SMO. (**c**) EKF robustness test against to electrical parameters. (**d**) EKF robustness test against to mechanical parameters. (**e**) SMO robustness test against electrical parameters. (**f**) EKF robustness test against to mechanical parameters.

In order to assess the performance of the observers offered as part of the electric vehicle application, the robust control diagram fitted with these observers was tested with a standardized driving cycle as a speed reference, which is the New European Driving Cycle (NEDC). The experimental results following this test are presented in Figure 10. This figure shows that the objective of the sensorless control is achieved. The obtained performances are very satisfactory, both in steady and transient conditions.

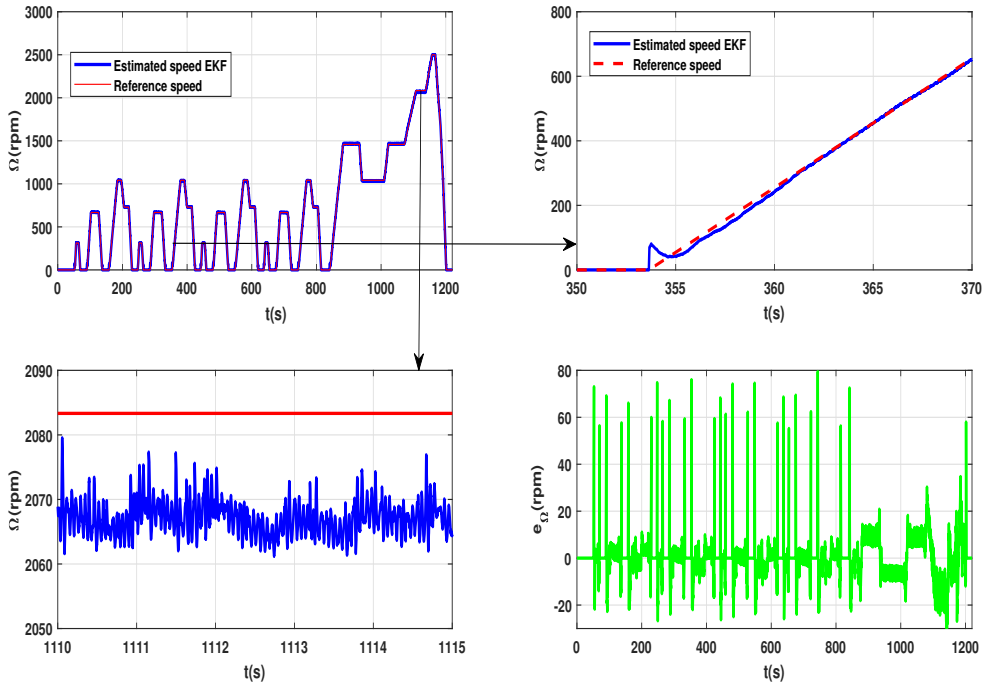

(**a**)

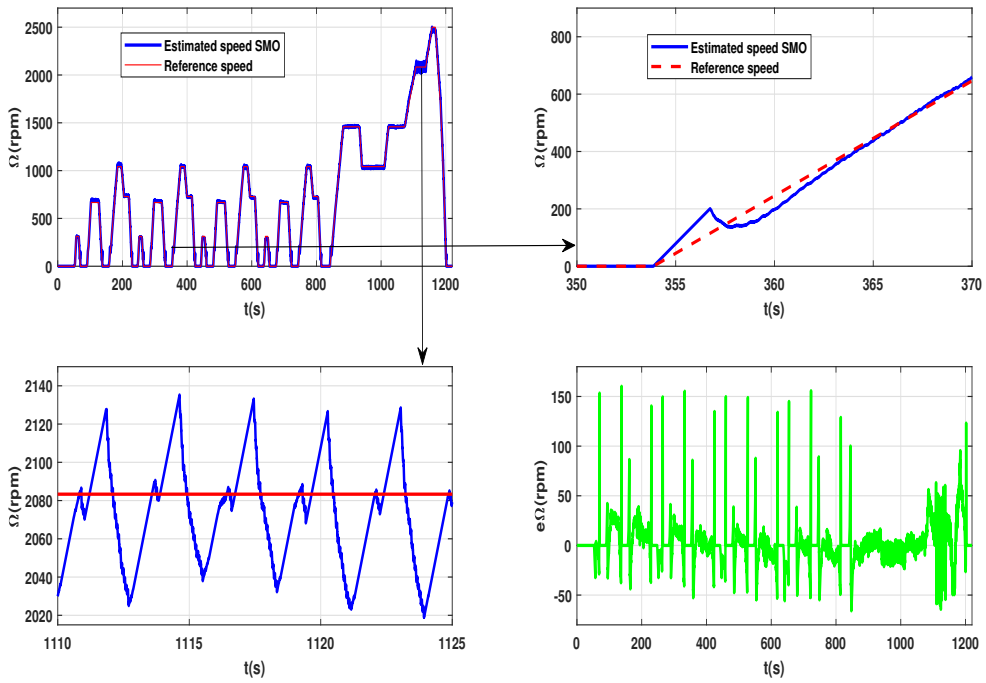

(**b**)

Figure 10. SRM tracking speed NEDC profile by EKF and SMO. (**a**) Speed tracking estimation by EKF. (**b**) Speed tracking estimation by SMO.

Table 1. Relative error of the estimated speed.

Observer Type	Relative Error at Low Speed	Relative Error at Medium Speed	Relative Error at High Speed
Sliding mode observer	0.1%	0 .2%	2%
Extended Kalman Filter	3%	0.15%	0.1%

5. Conclusions

This work is dedicated to the presentation of our contributions on robust control approaches coupled with the sensorless schemes for Switched Reluctance Motor (SRM) in case of electric vehicle applications. The cost of the mechanical sensor, its vulnerability and the loss of its reliability, led us to deal with the sensorless control approach.

Indeed, the contribution of this paper is how to counteract sensor reliability problems in harsh environments, the complexity, and the expensive cost to the system. Therefore, the designing of a full state observers (both position and speed estimation) is a necessary step for control tracking, diagnosis, and other Fault tolerant control (FTC) design problems. For such needs, we opted for two observers, the first one was the Extended Kalman Filter and the second one was based on Sliding Mode Observer (SMO). These observers are renowned for their robustness towards parametric uncertainties and external disturbances.

Experimental tests were carried out on a four phase SR motor prototype to prove the effectiveness of the sesorless architectures. Moreover, a robustness test of the control scheme has been performed. These observers were still able to build the estimated speed and rotor position under both mechanical and electrical parameter variations and against load torque variations. Through the experimental tests, the speed estimation built by SMO observer was better than the EKF speed estimation at low speed, while the EKF was suitably efficient for the medium and high speed range.

In future works, the aim is to extend the study in order to take into account the sensorless control during braking and very low speed operation of the electric vehicle, as well as to propose one or more new sensor fault tolerant strategies based on modern approach control theory.

Author Contributions: A.C., M.B., and N.O. developed the sensorless scheme, carried out the experimentation, and generated the results; A.C. and M.B. analyzed the results and were responsible for writing the paper, the research, reviewed the approach and the results to further improve the quality of the paper. E.M. reviewed and edited the paper. All authors have read and agreed to the published version of the manuscript.

Funding: This research received no external funding.

Conflicts of Interest: The authors declare no conflict of interest.

Nomenclature

SRM modeling parameters:

Notation	Definition	Unit
N	Number of phases	$j = 1 \ldots N = 4$
N_r	Number of rotor poles	*6*
i_j	Phase current	*A*
V_j	Phase winding voltage	*V*
R	Ohmic resistance of the phase	*Ohm*
L_j	Self inductance of the *j* phase	*H*
E	Back e.m.f	*V*
W_c	Co-energy	*J*
θ	Rotor angular position	*rad*
Ω	Angular speed	*rad/s*
T	Electromagntic torque	*N.m*
T_L	Load torque	*N.m*
f	Friction coefficient	$N.m.rad^{-1}.s$
J	Moment of inertia	$kg.m^2$
ϕ	flux linkage	*Wb*

Appendix A

$$a_{11} = 1 - T_s\left(\frac{i_1\frac{\partial L_{inc_1}}{\partial i_1} - L_{inc_1}}{L_{inc_1}^2}R - \frac{\frac{\partial L_{inc_1}}{\partial i_1}}{L_{inc_1}^2}V_1 + \frac{\frac{\partial}{\partial i_1}\left(\frac{\partial \phi_1}{\partial \theta}\right)L_{inc_1} - \frac{\partial \phi_1}{\partial \theta}\frac{\partial L_{inc_1}}{\partial i_1}}{L_{inc_1}^2}\Omega\right)$$

$$a_{12} = a_{13} = a_{14} = a_{17} = 0$$

$$a_{15} = -T_s\left(\frac{\frac{\partial \phi_1}{\partial \theta}}{L_{inc_1}}\right)$$

$$a_{16} = -T_s\left(-\frac{\frac{\partial L_{inc_1}}{\partial \theta}i_1}{L_{inc_1}^2}R + \frac{\frac{\partial L_{inc_1}}{\partial \theta}}{L_{inc_1}^2}V_1 + \frac{\frac{\partial}{\partial \theta}\left(\frac{\partial \phi_1}{\partial \theta}\right)L_{inc_1} - \frac{\partial \phi_1}{\partial \theta}\frac{\partial L_{inc_1}}{\partial \theta}}{L_{inc_1}^2}\Omega\right)$$

$$a_{21} = a_{23} = a_{24} = a_{27} = 0$$

$$a_{22} = 1 - T_s\left(\frac{L_{inc_2} - i_1\frac{\partial L_{inc_2}}{\partial i_2}}{L_{inc_2}^2}R - \frac{\frac{\partial L_{inc_2}}{\partial i_2}}{L_{inc_2}^2}V_2 + \frac{\frac{\partial}{\partial i_2}\left(\frac{\partial \phi_2}{\partial \theta}\right)L_{inc_2} - \frac{\partial \phi_2}{\partial \theta}\frac{\partial L_{inc_2}}{\partial i_2}}{L_{inc_2}^2}\Omega\right)$$

$$a_{25} = -T_s\left(\frac{\frac{\partial \phi_2}{\partial \theta}}{L_{inc_2}}\right)$$

$$a_{26} = -T_s\left(-\frac{\frac{\partial L_{inc_2}}{\partial \theta}i_2}{L_{inc_2}^2}R + \frac{\frac{\partial L_{inc_2}}{\partial \theta}}{L_{inc_2}^2}V_2 + \frac{\frac{\partial}{\partial \theta}\left(\frac{\partial \phi_2}{\partial \theta}\right)L_{inc_2} - \frac{\partial \phi_2}{\partial \theta}\frac{\partial L_{inc_2}}{\partial \theta}}{L_{inc_2}^2}\Omega\right)$$

$$a_{31} = a_{32} = a_{34} = a_{37} = 0$$

$$a_{33} = 1 - T_s\left(\frac{L_{inc_3} - i_4\frac{\partial L_{inc_3}}{\partial i_3}}{L_{inc_3}^2}R - \frac{\frac{\partial L_{inc_3}}{\partial i_3}}{L_{inc_3}^2}V_3 + \frac{\frac{\partial}{\partial i_3}\left(\frac{\partial \phi_3}{\partial \theta}\right)L_{inc_3} - \frac{\partial \phi_3}{\partial \theta}\frac{\partial L_{inc_3}}{\partial i_3}}{L_{inc_3}^2}\Omega\right)$$

$$a_{35} = -T_s\left(\frac{\frac{\partial \phi_3}{\partial \theta}}{L_{inc_3}}\right)$$

$$a_{36} = -T_s\left(-\frac{\frac{\partial L_{inc_3}}{\partial \theta}i_3}{L_{inc_2}^2}R + \frac{\frac{\partial L_{inc_3}}{\partial \theta}}{L_{inc_2}^2}V_3 + \frac{\frac{\partial}{\partial \theta}\left(\frac{\partial \phi_3}{\partial \theta}\right)L_{inc_3} - \frac{\partial \phi_3}{\partial \theta}\frac{\partial L_{inc_3}}{\partial \theta}}{L_{inc_3}^2}\Omega\right)$$

$$a_{41} = a_{42} = a_{43} = a_{47} = 0$$

$$a_{44} = 1 - T_s\left(\frac{L_{inc_4} - i_4\frac{\partial L_{inc_4}}{\partial i_4}}{L_{inc_4}^2}R - \frac{\frac{\partial L_{inc_4}}{\partial i_4}}{L_{inc_4}^2}V_4 + \frac{\frac{\partial}{\partial i_4}\left(\frac{\partial \phi_4}{\partial \theta}\right)L_{inc_4} - \frac{\partial \phi_4}{\partial \theta}\frac{\partial L_{inc_4}}{\partial i_4}}{L_{inc_4}^2}\Omega\right)$$

$$a_{45} = -T_s\left(\frac{\frac{\partial \phi_4}{\partial \theta}}{L_{inc_4}}\right)$$

$$a_{46} = -T_s\left(-\frac{\frac{\partial L_{inc_4}}{\partial \theta}i_4}{L_{inc_4}^2}R + \frac{\frac{\partial L_{inc_4}}{\partial \theta}}{L_{inc_4}^2}V_4 + \frac{\frac{\partial}{\partial \theta}\left(\frac{\partial \phi_4}{\partial \theta}\right)L_{inc_4} - \frac{\partial \phi_4}{\partial \theta}\frac{\partial L_{inc_4}}{\partial \theta}}{L_{inc_4}^2}\Omega\right)$$

$$a_{51} = \frac{T_s}{J}\left(\frac{\partial T_1}{\partial i_1}\right), a_{52} = \frac{T_s}{J}\left(\frac{\partial T_2}{\partial i_2}\right), a_{53} = \frac{T_s}{J}\left(\frac{\partial T_3}{\partial i_3}\right), a_{54} = \frac{T_s}{J}\left(\frac{\partial T_4}{\partial i_4}\right)$$

$$a_{55} = 1 - T_s\left(\frac{f_r}{J}\right), a_{56} = \frac{T_s}{J}\left(\frac{\partial T}{\partial \theta}\right), a_{57} = \frac{-T_s}{J}$$

$$a_{61} = a_{62} = a_{63} = a_{64} = a_{66} = a_{67} = 0, a_{65} = T_s$$
$$a_{71} = a_{72} = a_{73} = a_{74} = a_{75} = a_{76} = 0, a_{77} = 1.$$

$$B = \begin{bmatrix} \frac{T_s}{L_{inc_1}} & 0 & 0 & 0 \\ 0 & \frac{T_s}{L_{inc_2}} & 0 & 0 \\ 0 & 0 & \frac{T_s}{L_{inc_3}} & 0 \\ 0 & 0 & 0 & \frac{T_s}{L_{inc_4}} \\ 0 & 0 & 0 & 0 \\ 0 & 0 & 0 & 0 \\ 0 & 0 & 0 & 0 \end{bmatrix}, C = \begin{bmatrix} 1 & 0 & 0 & 0 & 0 & 0 & 0 \\ 0 & 1 & 0 & 0 & 0 & 0 & 0 \\ 0 & 0 & 1 & 0 & 0 & 0 & 0 \\ 0 & 0 & 0 & 1 & 0 & 0 & 0 \end{bmatrix}$$

References

1. Buerger, J.; Anderson, J. Robust control for electric vehicle powertrains. *Control Theory Technol.* **2019**, *17*, 382–392 [CrossRef]
2. Ouddah, N.; Boukhnifer, M.; Raisemche, A. Two control energy management schemes for electrical hybrid vehicle. In Proceedings of the 10th IEEE International Multi-Conferences on Systems, Signals & Devices (SSD13), Hammamet, Tunisia, 18–21 March 2013.
3. Belhadi, M.; Krebs, G.; Marchand, C.; Hannoun, H.; Mininger, X. Evaluation of axial SRM for electric vehicle application, *Electr. Power Syst. Res.* **2017**, *148*, 155–161. [CrossRef]
4. Cheng, M.; Sun, L.; Giuseppe, B.; Song, L. Advanced Electrical Machines and Machine-Based Systems for Electric and Hybrid Vehicles. *Energies* **2015**, *8*, 9541–9564. [CrossRef]
5. Ortega, R; Sarr, A; Bobtsov, A; Bahri, I; Diallo, D. Adaptive state observers for sensorless control of switched reluctance motors. *Int. J. Robust Nonlinear Control* **2019**, *29*, 990–1006. [CrossRef]
6. Cai, H.; Wang, H.; Li, M.; Shen, S.; Feng, Y. Position Sensorless Control of Switched Reluctance Motor with Consideration of Magnetic Saturation Based on Phase-Inductance Intersection Points Information. *Energies* **2018**, *11*, 3517. [CrossRef]
7. Pasquesoone, G; Mikail, R.; Husain, I. Position Estimation at Starting and Lower Speed in Three-Phase Switched Reluctance Machines Using Pulse Injection and Two Thresholds. *IEEE Trans. Ind. Appl.* **2011**, *47*, 1724–1731. [CrossRef]
8. Henderson, M.I. A sensorless method for switched reluctance motors. In Proceedings of the 8th IET International Conference on Power Electronics, Machines and Drives (PEMD 2016), Glasgow, UK, 19–21 April 2016; pp. 1-6.
9. Khan, Y.A.; Verma, V. Novel speed estimation technique for vector-controlled switched reluctance motor drive. *IET Electr. Power Appl.* **2019**, *13*, 1193–1203. [CrossRef]
10. Brandstetter, P.; Krna, P. Sensorless control of switched reluctance motor using sliding mode observer. In Proceedings of the 2013 International Conference on Applied Electronics, Pilsen, Czech Republic, 10–12 September 2013.
11. S. Kumari and S. Ashok, Design of controller for speed regulation and reduction of torque ripple in 6/4 switched reluctance motor. In Proceedings of the IEEE International Conference on Intelligent Techniques in Control, Optimization and Signal Processing (INCOS), Srivilliputhur, India, 23–25 March 2017; pp. 1–6.
12. Ouddah, N.; Boukhnifer, M.; Chaibet, A.; Monmasson, E. Fixed structure H_∞ loop shaping control of switched reluctance motor for electrical vehicle. *Trans. IMACS Math. Comput. Simul.* **2016**, *130*, 124–141. [CrossRef]
13. Ouddah, N.; Boukhnifer, M.; Chaibet, A.; Monmasson, E.; Berthelot, E. Experimental Robust H_∞ Controller Design of Switched Reluctance Motor for Electrical Vehicle Application. In Proceedings of the IEEE Multi-conference on Systems and Control, Juan Les Antibes, France, 15–17 July 2014; pp. 217–223.
14. Ouddah, N.; Boukhnifer, M.; Chaibet, A. Monmasson E., Robust controller designs of switched reluctance motor for electrical vehicle, Control and Automation (MED). In Proceedings of the 22nd IEEE Mediterranean Conference of Control and Automation, Palermo, Italy, 16–19 June 2014; pp. 212–217.
15. Apkarian, P.; Noll, D. Nonsmooth H_∞ synthesis. *IEEE Trans. Autom. Control* **2006**, *51*, 71–86. [CrossRef]

16. Peng, F.; Ye, J.; Emadi, A.; Huang, Y. Position Sensorless Control of Switched Reluctance Motor Drives Based on Numerical Method, *IEEE Trans. Ind. Appl.* **2017**, *53*, 2159–2168. [CrossRef]
17. Lu, W.; Keyhani, A. Sensorless Control of Switched Reluctance Motors Using Sliding Mode Observers. In Proceedings of the International Electric Machines and Drives Conference, Cambridge, MA, USA, 17–20 June 2001.